DALTON
FULL PAPER

Complexes of the lanthanide metals (La–Nd, Sm–Lu) with hypophosphite and phosphite ligands: crystal structures of $[Ce(H_2PO_2)_3(H_2O)]$, $[Dy(H_2PO_2)_3]$ and $[Pr(H_2PO_2)(HPO_3)(H_2O)]\cdot H_2O$

Joanne A. Seddon, Andrew R. W. Jackson, Roman A. Kresiński * and Andrew W. G. Platt

School of Sciences, Staffordshire University, College Road, Stoke-on-Trent, Staffordshire, UK ST4 2DE. E-mail: sctrak@staffs.ac.uk

Received 5th October 1998, Accepted 29th April 1999

Reactions of lanthanide chlorides $LnCl_3$ with NaH_2PO_2 in aqueous solution afforded a series of complexes $[Ln(H_2PO_2)_3(H_2O)_n]$ (Ln = La–Tb, $n = 1$; Ce–Nd, Dy–Lu; $n = 0$) with members falling into at least four separate structural types. The crystal structures of members of two of these types, $[Ce(H_2PO_2)_3(H_2O)]$ and $[Dy(H_2PO_2)_3]$, have been determined for the first time, along with that of $[Pr(H_2PO_2)(HPO_3)(H_2O)]\cdot H_2O$, one of a new series of complexes $[Ln(H_2PO_2)(HPO_3)(H_2O)_n]\cdot nH_2O$ (Ln = La–Gd, $n = 1$; Tb–Lu; $n = 0$) obtained by controlled oxidation of $[Ln(H_2PO_2)_3(H_2O)_n]$. The hydrated members of this series are notable due to their incorporation of chiral channels inhabited by water molecules, and to their ability reversibly to dehydrate. Steric angle sum calculations have been used to rationalise the morphologies of the new complexes.

Tripositive lanthanide ions are influenced only slightly by their own d or f orbitals in their bonding with ligands, these interactions being largely electrostatic. Others[1] have expounded from this that the concept of co-ordination saturation becomes equated with one of steric saturation in the case of lanthanide complexes. Thus, a wide variety of physicochemical properties of lanthanide complexes can vary smoothly when surveyed across the lanthanide series, until, at a certain limit, an abrupt variation is encountered.[2] This phenomenon is ascribable to the ionic radius of the lanthanide metal decreasing smoothly up to a point where the metal environment is sufficiently crowded as to eject one or more ligand atoms from the primary co-ordination sphere.

In a desire to survey systematically the structures of a family of simple lanthanide ion complexes we sought a ligand system which was uncomplicated, but nonetheless relatively unexplored, and this prompted our study of hypophosphite (phosphinate) complexes of lanthanides. Hypophosphite-containing structures appear to be well distributed around the Periodic Table: structures reported to date include those of d-block,[3–5] s-block,[6–9] p-block,[10,11] and actinide metals,[12,13] and an early structure of hypophosphite as its ammonium salt.[14] These show the hypophosphite ion to be very flexible in its co-ordination, doubly bridging[11,13] $\mu(\kappa^1,\kappa^1)$, triply bridging[3,5] $\mu_3(\kappa^1,\kappa^1,\kappa^1)$, and quadruply bridging[4,6] $\mu_4(\kappa^1,\kappa^1,\kappa^1,\kappa^1)$ modes all being represented.

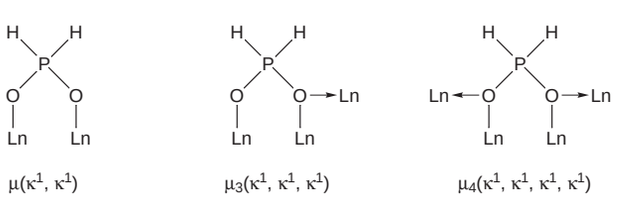

$\mu(\kappa^1, \kappa^1)$ $\mu_3(\kappa^1, \kappa^1, \kappa^1)$ $\mu_4(\kappa^1, \kappa^1, \kappa^1, \kappa^1)$

Four structures of lanthanide hypophosphite complexes have been elucidated to date. These are consistent with the expectation that later lanthanide ions should be less able to accommodate high co-ordination numbers than the larger, earlier lanthanides. Thus, the closely related complexes $[La(H_2PO_2)_3(H_2O)]$ and $[Eu(H_2PO_2)_3(H_2O)]$, belonging to structural types denoted by us here as **A** and **A′** respectively, accommodate a water ligand in their co-ordination spheres.[15,16] Two of the hypophosphite ligands adopt the $\mu(\kappa^1,\kappa^1)$ mode and the third $\mu_3(\kappa^1,\kappa^1,\kappa^1)$, the co-ordination number thus being eight in both structures. Despite their evident close similarity, the **A** and **A′** structures differ in the disposition of the $\mu_3(\kappa^1,\kappa^1,\kappa^1)$ ligand, and therefore cannot be considered isostructural.[16] The transition point between them in the lanthanide series has not yet been located and, in planning so to do, we considered that the close similarity of these structural types may prohibit unambiguous attribution of class to intervening lanthanide analogues simply by means of spectroscopic techniques. We anticipated that powder X-ray diffraction and, given the ability to grow suitable crystals, single-crystal X-ray diffraction, would prove our most valuable tools in achieving this and our other aims, which also include establishing for which metals anhydrous structural types may be formed. An example is the recently discovered[17] structural type **B** adopted by $[Pr(H_2PO_2)_3]$, which achieves 8-co-ordination by use of the $\mu(\kappa^1,\kappa^1)$ mode for one ligand only, the other two being $\mu_3(\kappa^1,\kappa^1,\kappa^1)$. In contrast, the late lanthanide complex $[Er(H_2PO_2)_3]$ is reported[18] to be 6-co-ordinate, having an approximately octahedral geometry about the metal ion, all hypophosphite ligands adopting the $\mu(\kappa^1,\kappa^1)$ mode; this structure is denoted by us here as belonging to type **C**. Our final aim was to explore whether other lanthanide structures might adopt types **B**, **C**, or an entirely new structural form, potentially one adopting the comparatively rare[1] 7-co-ordination.

Results and discussion

Synthetic studies

The reaction of aqueous solutions of lanthanide chlorides with sodium hypophosphite gave rise to the corresponding lanthanide hypophosphites. The compounds are all poorly soluble in water, but dissolve in dilute HCl. Their spectroscopic and other properties, and subsequent structural studies (discussed below), showed that the compounds form four distinct series of structural types depending on the metal and the reaction conditions. These and their interconversions are summarised in Table 1. In some cases air oxidation results in the formation of

Table 1 Formation of the various classes of lanthanide hypophosphite complexes

	La	Ce	Pr	Nd	(Pm)	Sm	Eu	Gd	Tb	Dy	Ho	Er	Tm	Yb	Lu
A	√	√	√	√											
A′						√	√	√	√						
B		b	b	b											
C							c		c	√	√	√	√	√	√

√, Formed on mixing reagents; b, formed from type **A** by digestive dehydration; c, formed on forced dehydration of type **A′**.

phosphite, manifest in the ^{31}P NMR spectra of the praseodymium and neodymium products completely dissolved in aqueous HCl. This oxidation is suppressed by carrying out the reaction under nitrogen or by buffering the solution to pH 1.4.

Digestion of the type **A** complexes on a water-bath over one day leads to the formation of anhydrous type **B** complexes for Ce, Pr and Nd. Interestingly no type **B** complex is observed for lanthanum and the type **A′** compounds do not undergo similar reactions. On prolonged digestion open to the air well defined mixed hypophosphite–phosphite complexes are formed. Two distinct forms of the mixed complex are observed, type **1**, $[Ln(H_2PO_2)(HPO_3)(H_2O)]\cdot H_2O$ (Ln = Pr–Gd) and an anhydrous type **2**, $[Ln(H_2PO_2)(HPO_3)]$ (Ln = Tb–Lu), but we have never unambiguously identified the lanthanum and cerium type **1** analogues. Over prolonged periods evidence of further oxidation to phosphate is observed in the ^{31}P NMR spectra of solutions of the products which show, in addition to HPO_3^{2-} and $H_2PO_2^-$, a singlet due to PO_4^{3-}.

The substitution of lanthanide chlorides by the nitrates, whilst giving the same hypophosphite complexes, leads to the acceleration of the formation of type **1** and **2** materials; in these cases the oxidation of hypophosphite by nitrate was confirmed by the identification of the main gaseous nitrogen containing product as N_2O contaminated with smaller amounts of NO, the infrared spectrum of the gas collected from the reaction mixture being identical with that expected from the literature.[19] Of note here is the observation that the cerium type **B** complex does not easily appear to undergo oxidation under these conditions.

In view of the formation of anhydrous hypophosphites for the heavier lanthanides it seemed reasonable to suppose that at some point the type **A′** and type **C** structures might possess similar stabilities and thus be interconvertible. Indeed, reaction of $[Tb(H_2PO_2)_3(H_2O)]$, the last type **A′** complex, with refluxing $HC(OMe)_3$ gives a type **C** complex which is considerably more soluble in water than the other type **C** compounds and can be precipitated therefrom as type **A′** by the addition of acetone. When Ln = Eu a type **C** compound is also formed, which rapidly rehydrates in air.

Attempts to convert type **1** into type **2** materials by dehydration with $HC(OMe)_3$ have not been successful.

Spectroscopic and thermal studies

All type **A**, **A′**, **B** and **C** complexes produced possess spectral and thermal properties consistent with their known [15–18] structures. Thus the types **A** and **A′** have very similar infrared spectra. Both are indicative of the presence of two or more different types of hypophosphite environment, and the presence of water (Fig. 1). Types **A′** have only three P–H stretching bands, presumably due to overlap. Thermal analysis shows an endotherm at around 210 °C, associated with a loss of *ca.* 5% mass, and consistent in all cases with loss of water. At around 310 °C there is a further compound exothermic event, resulting in a further 2% loss of mass; infrared investigation of the gaseous products of this decomposition revealed that phosphine [20] is evolved, and we believe the change to be attributable to the known [21] disproportionation of hypophosphite, occurring concomitantly with its partial oxidation. Type **B** complexes possess infrared spectra indicative of the absence of water ligands and the presence of

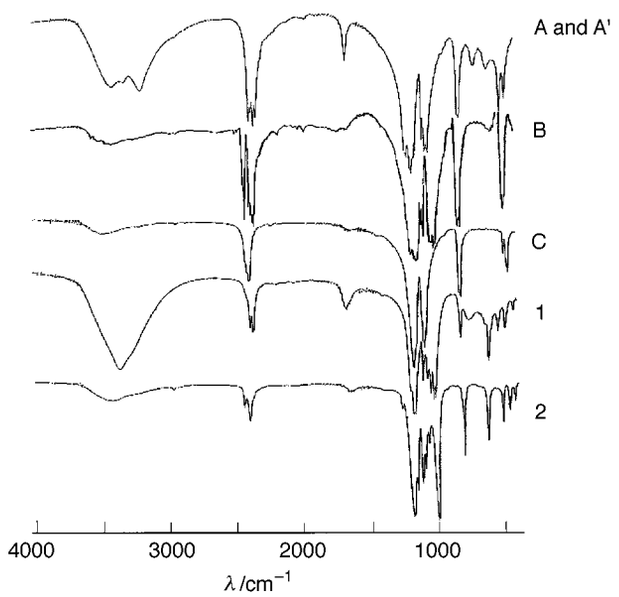

Fig. 1 Typical infrared spectra of all structural types.

two or more different types of hypophosphite. They lose no significant mass below 310 °C at which point an exothermic loss of 5% mass occurs. This is also attributable to the disproportionation of hypophosphite and, in common with the cases of **A** and **A′** above, is associated with another, concomitant, event, although much less in evidence here than in **A** or **A′**. Type **C** complexes possess uncomplicated infrared spectra indicative of rather uniform hypophosphite environments. They lose no significant mass below 340 °C, at which point there is an exothermic *gain* in mass of *ca.* 4% occurring over *ca.* 40 °C. Presumably this is air oxidation of hypophosphite, no loss of phosphine being observed; this fact can be rationalised by the structural studies discussed below. For all the above type **A**, **A′**, **B** and **C** complexes, their ^{31}P NMR spectra measured in aqueous HCl show only hypophosphite ion in solution.

Infrared spectra of the new type **1** complexes show intense broad bands in the appropriate regions indicating the presence of water. The P–H region is simple relative to type A complexes, but the P–O region is rather more complex. Thermal analysis reveals an endothermic loss of mass of *ca.* 11% at 130 °C, which corresponds to a loss of two water molecules per metal atom, followed by no further events up to 460 °C. Samples heated to 270 °C and allowed to stand in air appear to rehydrate to regenerate materials with type **1** infrared spectra. Most notably, however, ^{31}P NMR spectra of types **1** in aqueous HCl indicate the presence of both phosphite and hypophosphite, suggesting an empirical formulation of $Ln(H_2PO_2)(HPO_3)(H_2O)_2$ for type **1** complexes. Proton coupled ^{31}P NMR spectra of the complexes dissolved in concentrated HCl clearly show the presence of both phosphite (doublet) and hypophosphite (triplet). The integrated peak area ratios of these, measured using differing pulse delays and pulse widths, remains unaltered at 1 : 1, implying that rapid relaxation is occurring due to the presence of the paramagnetic lanthanide ions, and thus the measured ratio is a good reflection of the relative amounts of phosphite and hypo-

Table 2 Crystal data for lanthanide hypophosphite complexes

Formula	$[Ce(H_2PO_2)_3(H_2O)]$	$[Dy(H_2PO_2)_3]$	$[Pr(H_2PO_2)(HPO_3)(H_2O)]\cdot H_2O$
M	353.09	357.46	1287.62
Crystal system	Triclinic	Monoclinic	Orthorhombic
Space group	$P\bar{1}$	$C2/m$	$P2_12_12_1$
a/Å	7.1729(10)	14.368(3)	6.6558(5)
b/Å	7.9827(9)	5.7340(10)	7.1539(5)
c/Å	8.8710(6)	12.1230(10)	16.5506(18)
α/°	110.643(12)		
β/°	98.101(13)	122.33(2)	
γ/°	104.970(11)		
D_c/g cm^{-3}	2.642	2.813	2.713
Colour	None	Lilac	Light green
$F(000)$	334	660	608
Size/mm	0.20 × 0.25 × 0.30	0.35 × 0.24 × 0.24	0.25 × 0.28 × 0.30
θ Range/°	2.54–24.92	1.99–24.84	3.10–25.03
hkl ranges	$-8 \le h \le 5$, $-9 \le k \le 8$, $-10 \le l \le 10$	$-16 \le h \le 16$, $-6 \le k \le 5$, $-10 \le l \le 13$	$-7 \le h \le 7$, $-7 \le k \le 6$, $-18 \le l \le 17$
Total data	1964	1816	3274
Unique data	1274	717	1220
Merging R	0.0580	0.0495	0.0670
μ/mm^{-1}	5.661	9.398	6.574
t_{min}, t_{max}	0.532, 1.000	0.584, 1.000	0.740, 1.000
R (all data)	0.0374	0.0309	0.0430
$wR2$ (all data)	0.0922	0.0850	0.1029
Goodness of fit	1.112	1.129	1.051

phosphite present. The spectral properties of type **2** materials are similar to those of type **1** mentioned above, with the exception that no bands arising from water are evident in their infrared spectra. Their thermogravimetric traces are almost featureless below 460 °C. The infrared spectra of the materials obtained by thermal dehydration of type **1** complexes are very similar to those of type **2**, and we believe type **2** complexes to be the anhydrous analogues of type **1**, the absence of water being necessitated by smaller ionic radii of the later lanthanides, in the same way as type **C** are analogues of type **A** or **A′**. We therefore tentatively assign the formulation $Ln(H_2PO_2)(HPO_3)$ to type **2**. There is some evidence here of the existence of alternative structural types which might be denoted **1′** and **2′**, by analogy with **A′**. This arises from the interesting fact that type **1** materials when heated to 160 °C are completely dehydrated, and upon rehydration in air revert to type **1**. When heated to 270 °C, however, they possess different IR spectra after complete rehydration. These transformations are irreversible, but the products still contain the same 1 : 1 ratio of hypophosphite to phosphite (NMR evidence).

Structural studies

Powder X-ray diffraction patterns were simulated for all of types **A**, **A′**, **B** and **C** based upon the literature.[15–18] Experimental traces were recorded for all the new and known type **A**, **A′**, **B** and **C** complexes and showed four families of patterns, in accordance with the categories assigned to each complex by spectroscopic and thermal means. Good agreement was also obtained between each pattern prediction and the experimental trace in all cases, the worst fit being for types **C**. Patterns were also recorded for all type **1** materials, and also showed a familial resemblance. As a final verification of the compositions of these materials, and in order to clarify the discrepancy between the predicted and observed powder patterns of type **C** complexes, we sought to examine one of each type by single-crystal X-ray diffraction and found Ce to give satisfactory crystals of type **A**, Dy of **C**, and Pr of types **B** and **1**. No satisfactory crystals were obtained of any type **A′** complex except for Eu, or of any type **2** complex. Each of the above crystals afforded a structural solution. Details salient to data collection and structural refinement are presented in Table 2 (and elsewhere for $[Pr(H_2PO_2)_3]$).[17]

The structure of the cerium type **A** complex was confirmed to be $[Ce(H_2PO_2)_3(H_2O)]$ and is depicted in Fig. 2. It is, as indicated by supporting methods, virtually isostructural[15] with

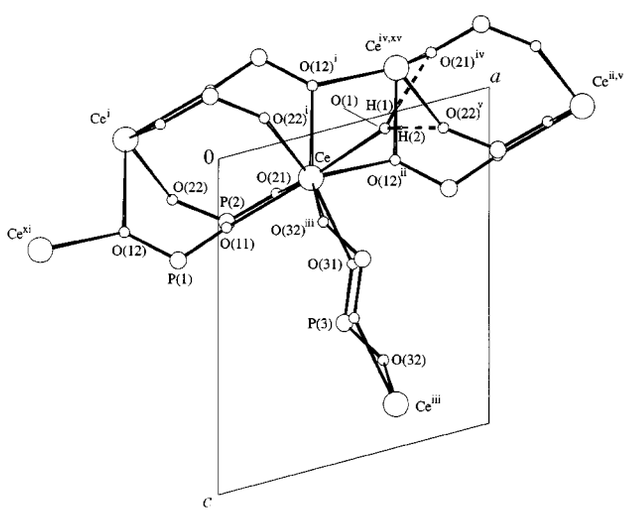

Fig. 2 A view[22] of $[Ce(H_2PO_2)_3(H_2O)]$ along the unit cell b axis. The Ce, P, O and H atoms are represented by spheres of decreasing relative arbitrary size. Only the water H atoms are shown, for reasons of clarity, along with their hydrogen-bonding contacts. Symmetry operators used throughout: $^{i} = -x, -y, -z$; $^{ii} = x + 1, y, z$; $^{iii} = 1 - x, 1 - y, 1 - z$; $^{iv} = 1 - x, -y, -z$; $^{v} = x + 1, y + 1, z$; $^{vi} = -x, -y, 1 - z$; $^{vii} = x, -y, z$; $^{viii} = x, 1 - y, z$; $^{ix} = 2 - x, y + \frac{1}{2}, \frac{1}{2} - z$; $^{x} = 2 - x, y - \frac{1}{2}, \frac{1}{2} - z$; $^{xi} = x - 1, y, z$; $^{xii} = x - \frac{1}{2}, 1\frac{1}{2} - y, -z$; $^{xiii} = 1\frac{1}{2} - x, 1 - y, z - \frac{1}{2}$; $^{xiv} = 1\frac{1}{2} - x, 2 - y, z - \frac{1}{2}$; $^{xv} = 1 - x, 1 - y, -z$; $^{xvi} = -x, y - 1, 1 - z$; $^{xvii} = x, y - 1, z$; $^{xviii} = -x, y, 1 - z$; $^{xix} = -x, 1 - y, 1 - z$; $^{xx} = -x, y - 1, -z$; $^{xxi} = -x, y, -z$; $^{xxii} = -x, 1 - y, -z$; $^{xxiii} = 1\frac{1}{2} - x, 1 - y, z + \frac{1}{2}$; $^{xxiv} = 1\frac{1}{2} - x, 2 - y, z + \frac{1}{2}$; $^{xxv} = x + \frac{1}{2}, 1\frac{1}{2} - y, -z$; $^{xxvi} = x, y + 1, z$.

$[La(H_2PO_2)_3(H_2O)]$, the structure of which is outlined briefly above. The Ln–O (hypophosphite) distance therein is 2.560[7] Å, but only 2.492[2] Å ($[\sigma_{mean}] = \sum_{i=1}^{i=n}(\sigma_i^2)/n$) in the cerium analogue (Table 3). There appears to be some compensation for this contraction in an extension of the hypophosphite ligands; the P–O (hypophosphite) lengths in $[Ce(H_2PO_2)_3(H_2O)]$ average 1.495[2] Å as compared with 1.478[6] Å in the lanthanum analogue, the O–P–O angles likewise extending to average 117.77[17]° as compared to 115.6[5]° in $[La(H_2PO_2)_3(H_2O)]$. The hydrogen atoms of the waters were not locateable, but their presence was inferred from two, and only two, close contacts between O(1) and hypophosphite atoms $O(21)^{iv}$ and $O(22)^{v}$ which subtend almost tetrahedral angles for $O(21)^{iv}\cdots O(1)$–Ce and $O(21)^{iv}\cdots O(1)\cdots O(22)^{v}$. The $O(22)^{v}\cdots O(1)$–Ce

Table 3 Selected interatomic separations (Å) and angles (°) for $[Ce(H_2PO_2)_3(H_2O)]$

Ce–O(11)	2.432(4)	Ce–O(21)	2.502(5)
Ce–O(31)	2.416(5)	Ce–O(1)	2.515(5)
Ce–O(12)^{i}	2.574(4)	Ce–O(12)^{ii}	2.607(4)
Ce–O(22)^{i}	2.482(5)	Ce–O(32)^{iii}	2.434(5)
P(1)–O(11)	1.483(5)	P(1)–O(12)	1.514(5)
P(2)–O(22)	1.496(5)	P(2)–O(21)	1.504(5)
P(3)–O(31)	1.484(5)	P(3)–O(32)	1.489(5)
O(1)···O(21)^{iv}	2.714(7)	O(1)···O(22)^{v}	2.834(7)
O(31)–Ce–O(11)	86.59(17)	O(31)–Ce–O(32)^{iii}	75.64(18)
O(11)–Ce–O(32)^{iii}	79.92(17)	O(31)–Ce–O(22)^{i}	150.06(18)
O(11)–Ce–O(22)^{i}	81.64(16)	O(32)^{iii}–Ce–O(22)^{i}	75.24(16)
O(31)–Ce–O(21)	78.99(18)	O(11)–Ce–O(21)	72.10(15)
O(32)^{iii}–Ce–O(21)	143.03(16)	O(22)^{i}–Ce–O(21)	122.41(15)
O(31)–Ce–O(1)	102.88(18)	O(11)–Ce–O(1)	146.97(16)
O(32)^{iii}–Ce–O(1)	72.20(17)	O(22)^{i}–Ce–O(1)	74.52(15)
O(21)–Ce–O(1)	140.46(15)	O(31)–Ce–O(12)^{i}	132.11(16)
O(11)–Ce–O(12)^{i}	119.21(15)	O(32)^{iii}–Ce–O(12)^{i}	143.38(15)
O(22)^{i}–Ce–O(12)^{ii}	77.19(15)	O(21)–Ce–O(12)^{i}	73.06(15)
O(1)–Ce–O(12)^{i}	77.56(15)	O(31)–Ce–O(12)^{ii}	71.36(15)
O(11)–Ce–O(12)^{ii}	144.17(15)	O(32)^{iii}–Ce–O(12)^{ii}	119.25(15)
O(22)^{i}–Ce–O(12)^{ii}	130.51(14)	O(21)–Ce–O(12)^{ii}	76.11(14)
O(1)–Ce–O(12)^{ii}	67.61(14)	O(12)^{i}–Ce–O(12)^{ii}	64.69(16)
O(11)–P(1)–O(12)	115.59(28)	O(22)–P(2)–O(21)	119.19(28)
O(31)–P(3)–O(32)	118.48(32)	Ce–O(1)···O(21)^{iv}	110.75(19)
Ce–O(1)···O(22)^{v}	142.04(22)	O(21)^{iv}···O(1)···O(22)^{v}	107.06(21)

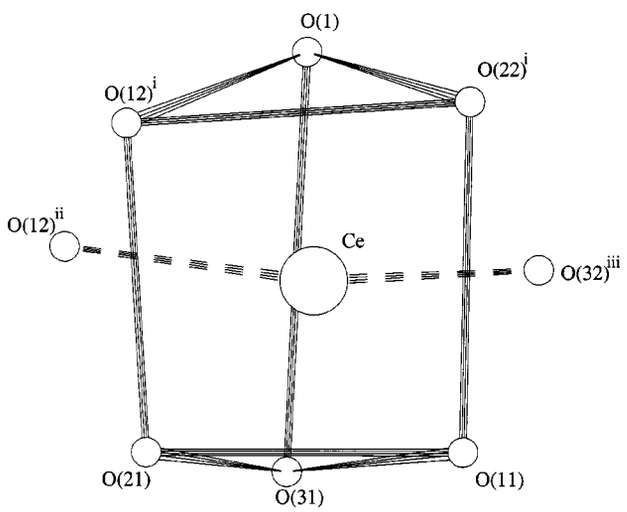

Fig. 3 The co-ordination polyhedron in $[Ce(H_2PO_2)_3(H_2O)]$.

angle, however, is far larger, which implies that, assuming an sp^3 hybridisation at O(1), the attitude of the lone pairs of O(1) to Ce is not one of direct alignment. This is, however, a common phenomenon, manifest also in other structures,[23–25] and probably implies a degree of interaction between Ce and both lone pairs; indeed, in this very structure, the orientations of the hypophosphite ligands also are not consistent with an sp^3 hybridisation at oxygen atoms and direct alignment between only one oxygen lone pair and Ce. The overall co-ordination geometry (Fig. 3) around Ce conforms most closely to bicapped trigonal prismatic (BTP), although polytopal analysis shape parameters[26] indicate that a degree of square antiprismatic (SAP) character is also present (Table 4; DOD = dodecahedral) which is manifest mainly in the elongation of the O(1)···O(31) distance so as to destroy the coplanarity of the sides of the prism.

The important bond distances and angles of the type **B** complex $[Pr(H_2PO_2)_3]$ have been communicated elsewhere.[17] Its overall co-ordination geometry conforms fairly closely to square antiprismatic (Table 4).

The structure reported[18] for $[Er(H_2PO_2)_3]$ and that determined by us for our dysprosium type **C** complex are different,

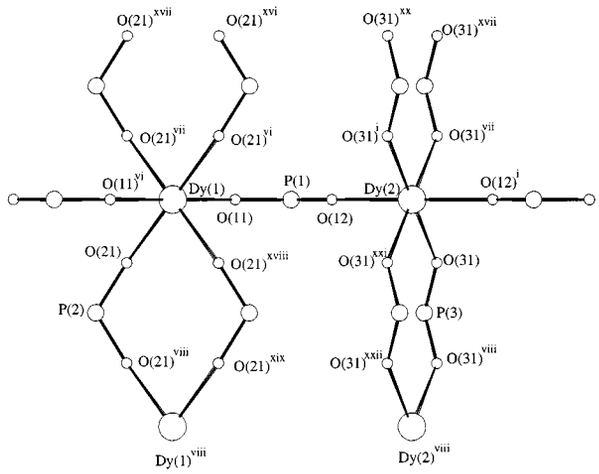

Fig. 4 A view[22] of $[Dy(H_2PO_2)_3]$. The Dy, P and O atoms are represented by spheres of decreasing relative arbitrary size, and H atoms are omitted.

but we note that the veracity of the former has been queried elsewhere.[23] Although the structures do not agree, the axial lengths of the two unit cells do, only the β angles being different. The two structures share the common characteristic of consisting a framework of metal atoms linked by $\mu(\kappa^1,\kappa^1)$-hypophosphite bridges extending along the principal axes of the lattice. The metal atoms (of which there are two crystallographically unique) in $[Dy(H_2PO_2)_3]$ are thereby six-co-ordinate. The co-ordination geometry is near-octahedral (Fig. 4), the *trans* angles being perfectly 180° and the *cis* angles ranging close around 90°, both extremes of this range being found at Dy(2). The mean Dy–O distance is 2.253[1] Å (Table 5), shorter than in any other lanthanide hypophosphite complex (leaving aside $[Er(H_2PO_2)_3]$).[18]

The presence of two waters per metal ion for the Type **1** complexes is substantiated by the emergent structure of $[Pr(H_2PO_2)(HPO_3)(H_2O)]\cdot H_2O$ (a formulation to be preferred over our former interpretation).[17] Only one of these waters is associated directly with the Pr. The metal is once again 8-co-ordinate by means of additional contributions from $\mu(\kappa^1,\kappa^1)$-hypophosphite and a $\mu_4(\kappa^2,\kappa^1,\kappa^1,\kappa^1)$-phosphite (Fig. 5).

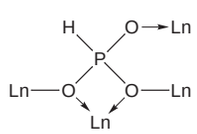

$\mu_4(\kappa^2, \kappa^1, \kappa^1, \kappa^1)$

As in $[Ce(H_2PO_2)_3(H_2O)]$, the water H atoms were not definitively located, but were clearly implied by interoxygen distances and angles: as a result it is clear that the structural units are bound together by means of the non-ligand water molecules, which bridge between hypophosphite O atoms as hydrogen-bonding acids, in turn acting as hydrogen-bonding bases to the ligand waters (Fig. 6). The result is a region of the structure inhabited by water molecules associated by hydrogen-bonding and extending along the screw axes. The space group itself being chiral, this area resembles a 'screw thread' of hydrogen bonds. Again, as in $[Ce(H_2PO_2)_3(H_2O)]$, the geometry at the ligand water is far from tetrahedral. The O(2)···O(1)···O(2)^{xii} angle is almost tetrahedral, but the corresponding angles between Pr and O(2) or O(2)^{xii} (these are the O atoms which act as hydrogen-bonding bases to H(13) and H(14) respectively) are obtuse; as in $[Ce(H_2PO_2)_3(H_2O)]$, no other close contacts are made with O(1) to imply a demand on the remaining lone pair, the implication being, in view of the angles at O(1), that it interacts somewhat with Pr. The geometry at O(2) is more regular (Table 6). The mean hypophosphite P–O

Table 4 Polytopal[a] analysis shape parameters for 8-co-ordinate lanthanide hypophosphite complexes

	$[Ce(H_2PO_2)_3(H_2O)]$	$[Pr(H_2PO_2)_3]$[b]	$[Pr(H_2PO_2)(HPO_3)(H_2O)]\cdot H_2O$	BTP	SAP	DOD
δ 1(57)3/°	13.8	8.0	34.1	21.8	0.0	29.5
δ 2(68)4/°	2.9	7.6	16.0	0.0	0.0	29.5
δ 2(58)3/°	45.6	50.0	50.7	48.2	52.5	29.5
δ 1(67)4/°	42.9	57.4	45.6	48.2	52.5	29.5
φ 7–1–2–8/°	16.0	24.2	5.1	14.1	24.5	0.0
φ 5–3–4–6/°	16.6	37.7	20.4	14.1	24.5	0.0

[a] Vertices are assigned, for the above three structures respectively, as follows: 1 [O(12)^{ii}, O(11), O(21)], 2 [O(21), O(21), O(22)], 3 [O(32)^{iii}, O(31), O(23)^{xi}], 4 [O(22)^{i}, O(12)^{xv}, O(1)], 5 [O(31), O(32)^{xix}, O(11)], 6 [O(12)^{i}, O(22)^{iv}, O(12)^{ix}], 7 [O(1), O(22), O(22)^{ix}], 8 [O(11), O(12)^{xi}, O(21)^{x}]. [b] See ref. 17.

Table 5 Selected interatomic separations (Å) and angles (°) for $[Dy(H_2PO_2)_3]$

Dy(1)–O(11)	2.243(6)	Dy(1)–O(21)	2.256(4)
Dy(2)–O(12)	2.246(6)	Dy(2)–O(31)	2.259(5)
P(1)–O(12)	1.439(7)	P(1)–O(11)	1.465(7)
P(2)–O(21)	1.486(5)	P(3)–O(31)	1.489(5)
O(11)–Dy(1)–O(21)	91.3(2)	O(11)–Dy(1)–O(21)^{vi}	88.7(2)
O(21)^{vi}–Dy(1)–O(21)^{vii}	89.5(2)	O(21)–Dy(1)–O(21)^{vii}	90.5(2)
O(11)–Dy(1)–O(11)^{vi}	180.0	O(21)–Dy(1)–O(21)^{vi}	180.0
O(12)–Dy(2)–O(31)	88.4(2)	O(12)^{i}–Dy(2)–O(31)	91.6(2)
O(31)–Dy(2)–O(31)^{vii}	90.1(2)	O(31)^{i}–Dy(2)–O(31)^{vii}	89.9(2)
O(12)^{i}–Dy(2)–O(12)	180.0	O(31)–Dy(2)–O(31)^{i}	180.0
O(12)–P(1)–O(11)	121.1(5)	O(21)–P(2)–O(21)^{viii}	116.6(4)
O(31)–P(3)–O(31)^{viii}	117.0(4)		

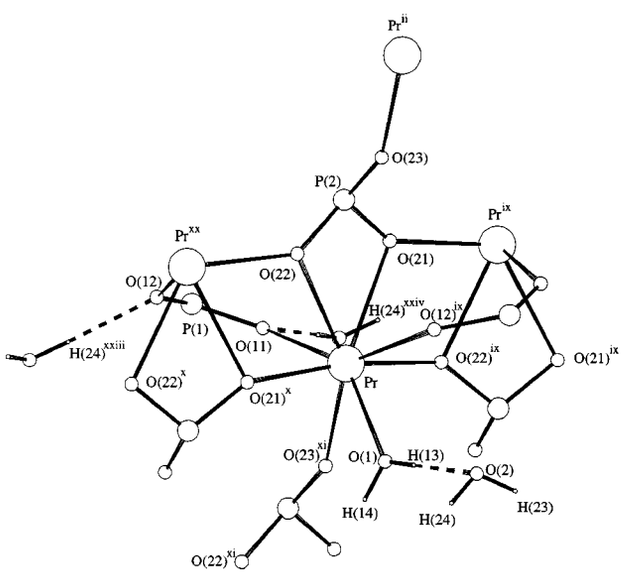

Fig. 5 A view[22] of $[Pr(H_2PO_2)(HPO_3)(H_2O)]\cdot H_2O$. The Pr, P, O and H atoms are depicted with decreasing arbitrary radii. Only H atoms, and their hydrogen-bonds to surrounding atoms, are shown for purposes of clarity.

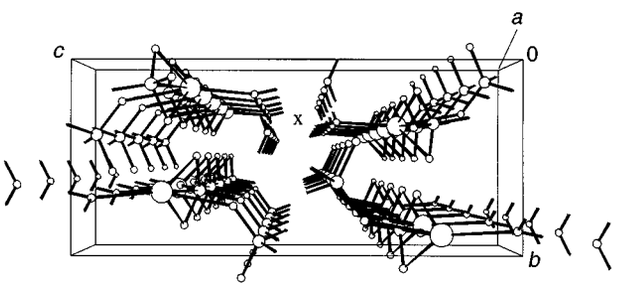

Fig. 6 The packing arrangement of $[Pr(H_2PO_2)(HPO_3)(H_2O)]\cdot H_2O$ seen[22] along the unit cell *a* axis. Some bonds are omitted for clarity. The symbol X denotes the approximate location of a screw axis consisting the centre of a 'screw thread' of water molecules.

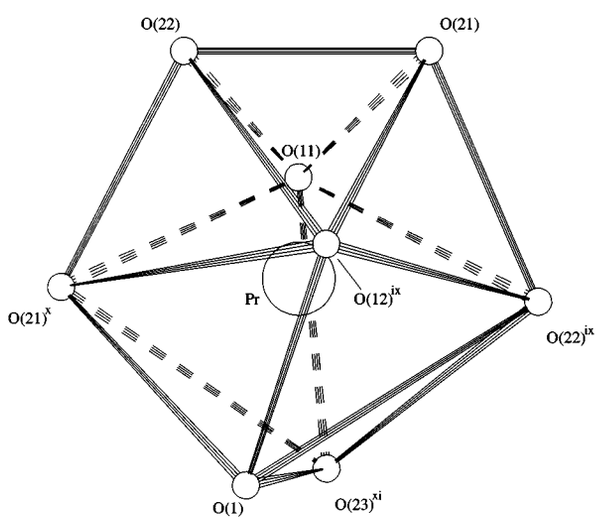

Fig. 7 The co-ordination around the Pr atom in $[Pr(H_2PO_2)(HPO_3)(H_2O)]\cdot H_2O$.

distance of 1.491[4] Å in this structure appears to be shorter than the 1.513[2] Å seen in $[Pr(H_2PO_2)_3]$, but this is to be interpreted in the light of the fact that both the co-ordination mode of the hypophosphites and the nature of the coligands is different in both structures. In the phosphite ligand the P(2)–O(23) distance is shorter than the distances to O(21) and O(22), which situation has been observed before[27,28] and is analogous to the asymmetry of the $\mu_3(\kappa^1,\kappa^1,\kappa^1)$-hypophosphite ligands, caused by different ligating demands on the two O atoms. In $[Pr(H_2PO_2)(HPO_3)(H_2O)]\cdot H_2O$ the co-ordination polyhedron is a dodecahedron, perhaps rather distorted in the direction of SAP by the loss of planarity of the O(11), O(23)^{xi}, O(1), O(12)^{ix} trapezoid (Fig. 7).

The degree of steric crowding in the above complexes can be compared by the use of steric angle sum (SAS) calculations,[1] which express the fraction of surface area of a notional 1 Å radius sphere, at a metal's centre, which is covered by conic projections of the ligating atoms. Computationally this is done by summing all of the individual atoms' contributions but, since overlap between the individual atoms' projections is not counted twice, an overlap correction is then applied. Values calculated for the above complexes are presented in Table 7 along with those for some related complexes. The table is arranged according to atomic weight of the metal, and the effects of the lanthanide contraction are immediately evident in the general increase in SAS values for the later lanthanides. The lanthanum complex has the smallest value, and there is no overlap correction required. In the case of the isostructural type **A** cerium complex a very small overlap correction is present, which arises from a close approach of atoms O(12)^{i} and O(12)^{ii} which reside in two $\mu_3(\kappa^1,\kappa^1,\kappa^1)$-hypophosphite ligands. This contact may be expected to become closer in the later lanthanide structures, and suggests that the structural change from **A** to **A**′ occurs when it reaches a limiting value. The SAS calculation for the type **A**′ $[Eu(H_2PO_2)_3(H_2O)]$ requires an overlap correction, but this arises mainly from a contact between the

Table 6 Selected interatomic separation (Å) and angles (°) for $[Pr(H_2PO_2)(HPO_3)(H_2O)]\cdot H_2O$

Pr–O(11)	2.479(6)	Pr–O(21)	2.639(6)
Pr–O(22)	2.570(5)	Pr–O(1)	2.475(7)
Pr–O(12)^{ix}	2.479(6)	Pr–O(21)^{x}	2.390(6)
Pr–O(22)^{ix}	2.395(5)	Pr–O(23)^{xi}	2.367(6)
P(1)–O(11)	1.478(6)	P(1)–O(12)	1.505(7)
P(2)–O(21)	1.540(6)	P(2)–O(22)	1.547(6)
P(2)–O(23)	1.490(6)	O(1)···O(2)	2.784(9)
O(1)···O(2)^{xii}	2.827(9)	O(2)···O(12)^{xiii}	2.794(8)
O(2)···O(11)^{xiv}	2.866(8)		
O(23)^{xi}–Pr–O(21)^{x}	90.82(20)	O(23)^{xi}–Pr–O(22)^{ix}	80.27(20)
O(21)^{x}–Pr–O(22)^{ix}	171.07(21)	O(23)^{xi}–Pr–O(1)	70.85(21)
O(21)^{x}–Pr–O(1)	79.98(23)	O(22)^{ix}–Pr–O(1)	96.31(23)
O(23)^{xi}–Pr–O(12)^{ix}	132.99(21)	O(21)^{x}–Pr–O(12)^{ix}	103.82(20)
O(22)^{ix}–Pr–O(12)^{ix}	82.07(20)	O(1)–Pr–O(12)^{ix}	68.29(21)
O(23)^{xi}–Pr–O(11)	77.29(23)	O(21)^{x}–Pr–O(11)	84.06(20)
O(22)^{ix}–Pr–O(11)	94.55(20)	O(1)–Pr–O(11)	143.93(23)
O(12)^{ix}–Pr–O(11)	147.52(21)	O(23)^{xi}–Pr–O(22)	147.80(19)
O(21)^{x}–Pr–O(22)	66.84(19)	O(22)^{ix}–Pr–O(22)	121.53(13)
O(1)–Pr–O(22)	123.70(22)	O(12)^{ix}–Pr–O(22)	76.93(20)
O(11)–Pr–O(22)	77.55(20)	O(23)^{xi}–Pr–O(21)	135.61(19)
O(21)^{x}–Pr–O(21)	122.41(15)	O(22)^{ix}–Pr–O(21)	65.63(18)
O(1)–Pr–O(21)	137.49(20)	O(12)^{ix}–Pr–O(21)	71.17(19)
O(11)–Pr–O(21)	77.99(22)	O(22)–Pr–O(21)	56.01(18)
O(11)–P(1)–O(12)	118.86(33)	O(23)–P(2)–O(21)	114.37(32)
O(23)–P(2)–O(22)	113.05(34)	O(21)–P(2)–O(22)	104.86(33)
Pr–O(1)···O(2)	133.35(30)	Pr–O(1)···O(2)^{xii}	123.82(27)
O(2)···O(1)···O(2)^{xii}	101.48(26)	O(1)···O(2)···O(12)^{xiii}	88.62(27)
O(1)···O(2)···O(11)^{xiv}	112.18(32)	O(11)^{xiv}···O(2)···O(12)^{xiii}	114.58(29)

Table 7 Steric angle sums (SASs) for lanthanide hypophosphite complexes

	SAS	
Complex	Uncorrected	Corrected
$[La(H_2PO_2)_3(H_2O)]$[a]	0.653	0.653
$[Ce(H_2PO_2)_3(H_2O)]$	0.691	0.691
$[Pr(H_2PO_2)_3]$[b]	0.698	0.698
$[Pr(H_2PO_2)(HPO_3)H_2O]\cdot H_2O$	0.705	0.699
$[Eu(H_2PO_2)_3(H_2O)]$[c]	0.738	0.733
$[Dy(H_2PO_2)_3]$	0.6503, 0.6486	0.6503, 0.6486

[a] See ref. 15. [b] See ref. 17. [c] See ref. 16.

$\mu_3(\kappa^1,\kappa^1,\kappa^1)$ and the water ligands, rather than between like ligands.

The type **B** $[Pr(H_2PO_2)_3]$ contains no strong contacts such as would necessitate an overlap correction, despite possessing a larger SAS value than $[Ce(H_2PO_2)_3(H_2O)]$ and being presumably more sterically crowded. The distribution of ligand atoms[17] around the metal ion in the type **B** materials is evidently quite efficient, which is in accordance with the observed SAP co-ordination geometry. This might explain why type **B** forms by dehydration of type **A**, even in the presence of water.

The complex $[Dy(H_2PO_2)_3]$ contains two crystallographically inequivalent dysprosium ions, and thus has two ascribable SAS values, the comparatively small magnitudes of which reflect the fact that this structure is a 6-co-ordinate one. This allows the ligands to move well away from one another, which is manifest in the lack of any overlap correction and the lower density of $[Dy(H_2PO_2)_3]$ compared to[17] $[Pr(H_2PO_2)_3]$. Furthermore, it might also afford type **C** complexes their resistance to disproportionation of hypophosphite, which occurs readily in types **A**, **A**′ and **B** at elevated temperatures. Since one of the products of this process is phosphine, interphosphorus oxygen transfer is a requisite, but there are no P···O approaches in $[Dy(H_2PO_2)_3]$ closer than 3.508(6) Å. This can be compared with values of 3.126(5) Å in $[Ce(H_2PO_2)_3(H_2O)]$ and 2.918(4) Å in $[Pr(H_2PO_2)_3]$, both of which fall well inside the sum of van der Waals radii of P and O for these type **A** and **B** complexes both of which undergo thermal disproportionation.

Conclusion

Whilst the hypophosphite–lanthanide system has not proven uncomplicated in its behaviour, relatively simple analyses, such as SAS calculations, appear to have afforded some fundamental insights to the structural preferences and reactivities of lanthanide hypophosphite complexes. These studies have established the classes of structures adopted by these materials and the ranges over which each is formed in the lanthanide series. The structure of type **A** has been verified by examination of a new member, and that of type **C** established correctly for the first time. No evidence for a 7-co-ordinate structural type, between the former 8- and the latter 6-co-ordinate complexes, has been found. A new class of mixed-ligand hypophosphite–phosphite complex, containing interesting chiral channels of water molecules, has been synthesized and characterised structurally.

Experimental

Instrumentation

JEOL JNM-FX270 and FX90Q (NMR), ATI Mattson Genesis single beam (FTIR) Philips 1050 Cu-Kα (powder diffraction) and Netzch STA 409 EP (TGA) instruments were used for routine analysis.

Analysis

Oxidisable phosphorus was determined by treatment of samples with an excess of bromine (generated quantitatively from bromate and bromide). The sample was stirred with bromine for 3 h in a stoppered flask, cooled in ice and an excess of potassium iodide added. The iodine liberated was titrated with standard sodium thiosulfate solution. For parity of reporting for pure hypophosphite and mixed-ligand systems, the results are expressed in terms of calculated molar mass. Percentage phosphorus values were determined by DCP (direct current plasma) atomic absorption spectroscopy.

Syntheses

$[Ln(H_2PO_2)_3(H_2O)_n]$ (types A and A′, $n = 1$; C, $n = 0$), general procedure. Sodium hypophosphite (*ca.* 1.00 g) was dissolved in pH 1.4 (KCl–HCl) buffer solution (10 ml). Hydrated lanthanide chloride (*ca.* 1.20 g) in the buffer solution (10 ml) was added. The mixture was allowed to stand in air at room temperature for one hour. A solid precipitated from solution where Ln = La–Eu, Dy–Lu. For Ln = Gd or Tb addition of a seed crystal resulted in rapid precipitation from the supersaturated solution. The resulting solids, bearing the characteristic colour of the Ln^{3+} ions, were collected by suction filtration, washed with water, and dried at the pump. Yields 61–89%. Representative analyses: $[Ce(H_2PO_2)_3(H_2O)]$, found P 26.1, $H_8CeO_7P_3$ requires 26.3%; $[Dy(H_2PO_2)_3]$, found P 25.6. $H_6DyO_6P_3$ requires 26.0%; $[Sm(H_2PO_2)_3(H_2O)]$, *M* found 366, theoretical 363; $[Eu(H_2PO_2)_3(H_2O)]$, *M* found 362, theoretical 365.

$[Ln(H_2PO_2)_3]$ (type B). Stoichiometric amounts of sodium hypophosphite and the lanthanide chloride were dissolved separately in the minimum amount of water. On mixing a precipitate was formed immediately, and the reaction mixture heated under reflux under nitrogen for several hours. Needle-like crystals formed of the colour of the corresponding Ln^{3+} ion, which were collected by suction filtration, washed with water, and dried at the pump. Yields 51–69%. $[Pr(H_2PO_2)_3]$, *M* found 336, theoretical 336.

$[Tb(H_2PO_2)_3]$ (type C) from $[Tb(H_2PO_2)_3(H_2O)]$ (type A′). A small quantity of $[Tb(H_2PO_2)_3(H_2O)]$ was stirred under reflux with excess of trimethyl orthoformate in a nitrogen atmosphere for 2 h. The resulting material was filtered in a dry-box, washed with dry thf and allowed to dry.

$[Ln(H_2PO_2)(HPO_3)(H_2O)_n]\cdot H_2O$ (type 1, $n = 1$; 2, $n = 0$). Air oxidation of the lanthanide hypophosphite complexes, monitored by IR spectroscopy, was achieved by *in situ* air oxidation on heating the lanthanide chloride with sodium hypophosphite in aqueous solution on a steam-bath for several hours. Needle like crystals were formed for the praseodymium and neodymium complex, whilst for the later lanthanides the complexes were obtained as fine powders. The products were filtered off, washed with water and dried in air at the pump. Representative analyses: $[Nd(H_2PO_2)(HPO_3)(H_2O)]\cdot H_2O$, *M* found 301, theoretical 325; $[Tm(H_2PO_2)(HPO_3)]$, *M* found 316, theoretical 314; $[Lu(H_2PO_2)(HPO_3)]$, *M* found 325, theoretical 320.

Crystallography

Diffraction data were collected, using Mo-Kα radiation, according to previously published procedures.[29] Non-H atoms were modelled[30] anisotropically, and H atoms isotropically, these being placed in theoretical positions. Following convergence of full-matrix least-squares refinement[30] using merged data, these were corrected[31] for absorption effects and refinement resumed to convergence.

$[Ce(H_2PO_2)_3(H_2O)]$. The structure was solved by isomorphous replacement.[15] A common refined P–H distance (1.309(14) Å) was used, and water H atoms were restrained to sit 30% along the length of their putative hydrogen-bonding vectors and, as a result, the refinement was unstable and required slight damping. Final error limits were estimated using undamped cycles of refinement. The largest hole and peak in the final Fourier-difference map were −1.08 and 1.40 e $Å^{-3}$ (at Ce).

$[Dy(H_2PO_2)_3]$. Data were collected as for triclinic symmetry, and transformed to the above system. The structure was solved by trial placement of heavy atoms at special positions. A common refined P–H distance (1.245(15) Å) was used for the refinement. The largest hole and peak in the final Fourier-difference map were −0.86 and 0.74 e $Å^{-3}$ (*ca.* 1.2 Å from Dy(1) and O(11)).

$[Pr(H_2PO_2)(HPO_3)(H_2O)]\cdot H_2O$. The structure was solved by Patterson methods.[32] A common refined P–H distance (1.266(26) Å) was used, which was considered a reasonable step in the light of the similarity of the IR stretching frequencies. Some systematic error in the data necessitated that phosphite O atoms be weakly restrained to be isotropic to prevent 'non-positive definite' collapse. Water H atoms were restrained to sit 30% along the length of their putative hydrogen-bonding vectors and, as a result, the refinement was unstable and required damping. Final error limits were estimated using undamped cycles of refinement. The largest hole and peak in the final Fourier-difference map were −1.29 and 3.99 e $Å^{-3}$ (at Pr).

CCDC reference number 186/1450.

Acknowledgements

The authors gratefully acknowledge the use of the EPSRC's X-Ray Crystallography Service, and Chemical Database Service at Daresbury. Thanks are due to Stephanie Barnett for simulations of powder patterns, and to all in the Divison of Ceramics for use of apparatus.

References

1 X.-Z. Zhang, A.-L. Guo, Y.-T. Xu, X.-F. Li and P.-N. Sun, *Polyhedron*, 1987, **6**, 1041.
2 F. A. Hart, in *Comprehensive Coordination Chemistry*, eds. G. Wilkinson, R. D. Gillard and J. A. McCleverty, Pergamon Press, Oxford, 1987, vol. 3.
3 M. D. Marcos, R. Ibanez, P. Amoros and A. LeBail, *Acta Crystallogr., Sect. C*, 1991, **47**, 1152.
4 T. J. R. Weakley, *Acta Crystallogr., Sect. B*, 1979, **35**, 42.
5 M. D. Marcos, P. Amoros, F. Sapina, A. Beltran-Porter, R. Martinez-Manez and J. P. Attfield, *Inorg. Chem.*, 1993, **32**, 5044.
6 T. Matsuzaki and Y. Itaka, *Acta Crystallogr., Sect. B*, 1969, **25**, 1932.
7 B. O. Loopstra, *Int. Estab. Nucl. Energy Res. Publ.*, 1958, **15**, 64.
8 A. R. Pedrazuela, S. Garcia-Blanco and L. Rivoir, *An. Soc. Esp. Fis. Quim.*, 1953, **49**, 255.
9 T. Akimoto, Ph.D. Thesis, University of Tokyo, 1965.
10 T. J. R. Weakley, *J. Chem. Soc. Pak.*, 1983, **5**, 279.
11 T. J. R. Weakley and W. W. L. Watt, *Acta Crystallogr., Sect. B*, 1979, **35**, 3023.
12 P. A. Tanner, T. Sze, T. C. Mak and W. Yip, *J. Cryst. Spectrosc. Res.*, 1992, **22**, 25.
13 P. A. Tanner, S.-T Hung, T. C. W. Mak and W. Ru-Ji, *Polyhedron*, 1992, **11**, 817.
14 W. H. Zachariasen and R. C. L. Mooney, *J. Chem. Phys.*, 1934, **2**, 34.
15 V. M. Ionov, L. A. Aslanov, V. B. Rybakov and M. A. Porai-Koshits, *Kristallografiya*, 1973, **18**, 403.
16 V. M. Ionov, L. A. Aslanov, M. A. Porai-Koshits and V. B. Rybakov, *Kristallografiya*, 1973, **18**, 405.
17 J. A. Seddon, A. R. W. Jackson, R. A. Kresinski and A. W. G. Platt, *Polyhedron*, 1996, **15**, 1899.
18 L. A. Aslanov, V. M. Ionov, M. A. Porai-Koshits, V. G. Lebedev, B. N. Kulikovskii, O. N. Gilyarov and T. L. Novoderezhkina, *Izv. Acad. Nauk. SSSR, Neorg. Mater.*, 1975, **11**, 96.
19 J. Laane and J. R. Ohlsen, *Prog. Inorg. Chem.*, 1980, **27**, 465.
20 K. Nakamoto, *Infrared and Raman Spectra of Inorganic and Coordination Compounds*, 4th edn., Wiley, New York, 1986.
21 J. W. Mellor, *Comprehensive Treatise on Inorganic and Theoretical Chemistry*, Longmans, New York, London, 1971, vol. 8, suppl. 3.
22 E. K. Davies, SNOOPI, Chemical Crystallography Laboratory, University of Oxford, 1982.
23 The United Kingdom Chemical Database Service, D. A Fletcher, R. F. McMeeking and D. Parkin, *J. Chem. Inf. Comput. Sci.*, 1996, **36**, 746.
24 D. L. Faithfull, J. M. Harrowfield, M. I. Ogden, B. W. Skelton, K. Third and A. H. White, *Aust. J. Chem.*, 1992, **45**, 583.
25 M. C. Favas, D. L. Kepert, B. W. Skelton and A. H. White, *J. Chem. Soc., Dalton Trans.*, 1980, 454.
26 M. A. Porai-Koshits and L. A. Aslanov, *J. Struct. Chem.*, 1978, **13**, 244.

27 Y.-P. Zhang, H. Hu and A. Clearfield, *Inorg. Chim. Acta*, 1992, **193**, 35.
28 J.-D. Foulon, N. Tijani, J. Durand, M. Rafiq and L. Cot, *Acta Crystallogr.*, *Sect. C*, 1993, **49**, 1.
29 J. A. Darr, S. R. Drake, M. B. Hursthouse and K. M. A. Malik, *Inorg. Chem.*, 1993, **32**, 5704.
30 G. M. Sheldrick, SHELXL 93, Program for Crystal Structure Refinement, University of Göttingen, 1993.
31 N. Walker and D. Stuart, *Acta Crystallogr.*, *Sect. A*, 1983, **39**, 158.
32 G. M. Sheldrick, SHELXS 86, Program for the Solution of Crystal Structures, University of Göttingen, 1986.

Paper 8/07727D